RSC Advances

ROYAL SOCIETY OF CHEMISTRY

www.rsc.org/advances

Chemical and Electrochemical Hydrogenation of CO_2 to hydrocarbons on Cu Single Crystal Surfaces: Insights into the Mechanism and Selectivity from DFT Calculations

Lihui Ou*

Abstract: Atomic level mechanistic insights into the chemical and electrochemical reduction of CO_2 on the Cu(111) and Cu(100) surfaces are presented based on DFT-based thermodynamic and kinetic calculations. On Cu(111), CO_{ads} is firstly formed by dissociative hydrogenation of CO_2, the CHO_{ads} and CH_2O_{ads} are the key intermediates towards the chemical and electrochemical reduction of CO_2 into methanol and CH_4. Despite of being the thermodynamics or kinetics, it is likely that CH_2OH_{ads} instead of CH_3O_{ads} is the intermediate for methanol and CH_4 formation. Based on the activation barriers, the CH_2OH_{ads} intermediate either forms CH_3OH by direct hydrogenation or forms CH_{2ads} by hydrogenative dissociation, which maybe a parallel path in CO_2 reduction mechanism on the Cu(111) surface, finally, the CH_2 intermediate lead to formation of the hydrocarbons. On Cu(100), CO_2 reduction takes a different pathway in the early stages, CO is formed through direct dissociation of CO_2 rather than hydrogenative dissociation as on the Cu(111) surface due to stronger bonding of CO, and CO further reduction also undergoes different pathway, in which CO dimerization is more easily to achieve, whereas CO hydrogenation is difficult to occur on the Cu(100) surface, explaining the unique selectivity for C_2H_4, namely, why C_2H_4 is formed more favorably on the Cu(100) surface and CH_4 is predominantly produced on the Cu(111) surface under both chemical and electrochemical conditions. Additionally, DFT calculated results showed for the first time that the electrochemical reduction would be expected to be highly favored at potentials of interest to CO_2 reduction compared with the chemical reduction and the carbon dioxide anion radical ($\cdot CO_2^-$) is involved in the initial stage of CO_2 electroreduction. Simultaneously, the results also explained partly why CH_3OH is formed in gas phase chemistry and only CH_4 is observed in electrochemistry on copper surfaces. By analyzing the chemical and electrochemical reduction paths, important mechanistic information is deduced on the Cu single crystal

College of Chemistry and Chemical Engineering, Hunan University of Arts and Science, Changde 415000, China.
** To whom correspondence should be addressed. E-mail: oulihui666@126.com.*
Phone: +86-736-7186115.

Electronic supplementary information (ESI) available.

surfaces. The study of CO_2 reduction mechanisms on copper will lead to a deeper understanding of the reaction chemistry and can eventually lead to the design of more efficient and selective catalysts.

Keywords: Density functional theory calculations; Carbon dioxide reduction; The minimum energy paths; Selectivity; Cu single crystal surface

1. Introduction

Converting CO_2 into organic fuels and/or chemicals would positively impact the global carbon balance and offer a novel solution to the dilemma of growing energy demand and global warming we are facing nowadays.[1, 2] Among various CO_2 fixation methods, reduction with hydrogen gas[3, 4] or electricity[1, 5-9] may represent the most promising pathways since that either of them can be generated on large scales by the sustainable energies such as solar, hydro and wind, thus in the mean time providing a way for storing these intermittently available sustainable energies. The two reduction methods similarly involve successive hydrogenation of CO_2 molecules, leading to a variety of products such as formic acid, methanol and hydrocarbons. In comparison, the electrochemical reduction of CO_2 offers several advantages such as room temperature and ambient pressure operation, tunable reaction rate and selectivity by electrode potential, and capability of producing hydrocarbons such as methane (CH_4) and ethylene (C_2H_4),[1, 5-9, 10-13] which are particularly desired due to their high energy densities and widespread use in the current energy and industrial infrastructures. Among electrocatalyst materials so far explored, metallic Cu is most capable of converting CO_2 into hydrocarbons with high faraday efficiency.[5, 7, 8, 10-19] Therefore, the electrochemical reduction of CO_2 on Cu-based materials has received growing interests in recent years.

Although CO_2 can be converted into CH_4 and C_2H_4 with high faraday efficiency on Cu electrodes, considerable overpotentials are required for the reaction to occur, with the onset potentials being around -0.7 V and -0.8 V (*vs* RHE) respectively for the formation of C_2H_4 and CH_4.[5-7, 20] At less negative potentials, formate and CO are the main products. Studies on single crystal surfaces showed that on the Cu(100) surface more C_2H_4 was formed whereas the Cu(111) surface produced more CH_4.[7, 21, 22] Understanding the atomic-level origin of the product distribution and the surface structure effect in CO_2 electroreduction is crucial for electrocatalyst optimization. This requires a detailed microscopic view on the reaction pathways and kinetics. It has been found that the electroreduction of CO exhibits very similar potential and surface structure dependence of the CH_4 and C_2H_4 formation, while experiments starting with HCOOH showed no detectable products,[20, 23] which indicated that the CO is one of the intermediate involved in CO_2 electroreduction to these hydrocarbons and CO is formed in a separate pathway from formate formation.[8, 13, 21, 24, 25] However, the reaction pathways and intermediates following CO formation remain unclear.

Based on the reaction free energies calculated using density functional theory (DFT) for various possible elementary steps, Nørskov and coworkers[11, 12] recently proposed that the formation of CH_4 and C_2H_4 from CO_2 on various fcc Cu facets similarly involve the hydrogenative reduction of CO to an adsorbed formyl (CHO*) as the rate-determining step (rds), which is followed by successive hydrogenative reduction

steps to form adsorbed formaldehyde (CH_2O*) and methoxy species (CH_3O).[11] However, experimental results obtained recently by Koper and coworkers[16] and earlier by Hori et al[25] seemed to suggest that the reaction paths of CH_4 and C_2H_4 formation are separated at an early stage of CO reduction. Results from a more recent experiment study of CO electroeduction on single-crystal copper electrodes by Koper and coworkers[21] further implied that there are two separate pathways for the C_2H_4 formation: one that shares an intermediate with the pathway to CH_4 and one that occurs mainly on Cu(100) and probably involves the formation of a CO dimmer as the key intermediate.[8] The latest DFT calculation study by Nie et al[19] suggested an alternative reaction path in which both CH_4 and C_2H_4 production through a hydroxymethylidyne (COH) intermediate from CO electroreduction. These controversial results and propositions have left both the rate-determining and selectivity-determining steps for the formation of hydrocarbon products from CO_2 and CO electroreduction on Cu still uncertain. As well, several other questions in the reaction mechanism remain, such as, why methanol that is the dominant product on copper catalysts in chemical reduction is nearly absent in the electrochemical reduction, whether methylene ($:CH_2$) proposed in earlier studies[8] is involved in the hydrocarbon formation, and why C_2H_4 formation is favored over CH_4 at lower overpotentials, etc.

In an attempt to gain the dominant reaction pathways for the formation of various products in CO_2 reduction, we present a systematic DFT calculation on the reaction free energies and the activation barriers of various possible elementary steps on the two most common types of Cu surfaces, namely, the closed-packed Cu(111) surface and the open Cu(100) surface. Both the chemical reduction by gaseous hydrogen and the electrochemical reduction through proton-electron pair are considered and their similarities and distinctness are discussed. We calculated the free energies of reaction and the activation barrier for the chemical reduction, according to which the optimized pathways for chemical reduction are deduced. With the theoretical hydrogen electrode model, the effect of electrode potentials on the steps in these pathways is discussed. Based on the calculated reaction free energy, the pathways in which the water in the double layer as the hydrogenation agent in electrochemical environment are discussed. The mechanism of the electrochemical reduction is proposed. In chemical reduction, the adsorbed hydrogen atoms (H*) should be the main reducing and hydrogenation agent, while in electrochemical reduction the hydrogenative reduction can be either accomplished by H* or by proton from the double layer plus electron from electrode. In thermodynamics, the two ways are not distinguished, but they could be different kinetically due to that the transition states in the two cases could be totally different.

2. Computational method and modeling

Calculations were performed in the framework of DFT using the generalized gradient approximation (GGA) of Perdew-Burke-Ernzerhof (PBE)[26] and employing ultrasoft pseudopotentials[27] for Nuclei and core electrons. The calculations of reaction free energies were performed using periodic super-cells with the Cu electrodes modeled by four-layer slabs with a 3×3 surface. A vacuum space of 16Å was placed above the slabs and adsorption is allowed on only one of the two surfaces exposed. The Kohn-Sham orbitals were expanded in a plane-wave basis set with a kinetic energy cutoff of 26 Ry and the charge-density cutoff of 260 Ry. The Fermi-surface effects was treated by the smearing technique of Methfessel and Paxton, using a smearing parameter[28] of 0.02 Ry. Calculations were carried out with spin-polarization, which is essential to properly represent the electronic structure of adsorbed CO_2. The PWSCF codes contained in the Quantum ESPRESSO distribution[29] were used to implement all calculations, while figures of the chemical structures were produced with the XCRYSDEN[30-32] graphical package. BZ integrations were performed using a (3×3×1) uniformly shifted k-mesh for (3×3) supercell.

The calculated equilibrium lattice constant for Cu was 3.66Å, which agreed well with theoretical and experimental values (3.66 and 3.62Å, respectively).[33, 34] During the calculations, the structure of the bottom two layers were fixed at the theoretical bulk positions, whereas the top two layers and the adsorbates were allowed to relax and all the other structural parameters were optimized so as to minimize the total energy of the system. Structural optimization was performed until the Cartesian force components acting on each atom were brought below 10^{-3} Ry/Bohr and the total energy converged to within 10^{-5} Ry.

The climbing-image nudged elastic band (CI-NEB) method was used to determine the minimum energy paths (MEPs) for all the elementary steps.[35, 36] The transition state of the optimized reaction coordinate was approximated by the image of highest energy. The transition state images from the CI-NEB calculations were optimized using the quasi-Newton method, which minimizes the forces to find the saddle point. Geometry optimization was performed for each intermediate point in MEPs, in which a three-layer Cu slab with a 2×3 surface unit cell was used considering the high cost of CI-NEB calculation, the bottom two layers of metal atoms were fixed while the top layer of metal atoms and all other nonmetal atoms were allowed to relax.

The adsorption energy (E_{ad}) of adsorbate "A" was calculated according to $E_{ad}(A) = E(\text{slab-A}) - E(\text{slab}) - E(A)$, where E(slab-A), E(slab) and E(A) refer to the total energy of a slab with an adsorbed "A", the total energy of a slab, and the total energy of the free "A" respectively. The co-adsorption energy between adsorbates "A" and "B" was calculated according to $E_{ad}(A, B) = E(\text{slab-A, B}) - E(\text{slab}) - E(A) - E(B)$, in which E(slab-A, B) refers to the calculated total energy of the slab with co-adsorbed "A" and "B". The

difference value of "E_{ad}(A, B) − (E_{ad}(A) + E_{ad}(B))" should represent the interaction between "A" and "B" on the surface.

3. Results and discussion

3.1 Chemical reduction of CO_2

Table 1 lists the possible reaction steps in the chemical reduction of CO_2 by H_2 and the DFT-calculated reaction free energies for these steps on the Cu(111) and Cu(100) surfaces. The preferred adsorption configurations for all the reactants, intermediates and products listed in Table 1 on the two surfaces are given in Table S1, S2, S3, S4, S5 and S6, and Figures S1, S2 and S3 in the Supporting Information (SI). For the sake of simplicity, we directly use H_2 molecule as the reactant in the reaction free energy calculations for all the hydrogenation steps. In reality, the hydrogenation agent in the elementary reaction steps of chemical reduction should be the adsorbed hydrogen atoms (H*) formed through H_2 dissociation. Therefore, the hydrogenation steps listed in Table 1 are not the elementary reaction steps. Although they are not the elementary steps, the calculated reaction free energies in Table 1 should still represent the general thermodynamic preference of various hydrogenation steps.

According to calculated adsorption free energies (Table S1), CO_2 can not form stable chemical adsorption states on the Cu(111) and Cu(100) surfaces. Therefore, the gaseous CO_2 is used in the free energy calculations. Physisorption state of CH_4 and chemisorption state of C_2H_4 is obtained on the Cu(111) surface. The corresponding adsorbed states of CH_4 and C_2H_4 are also obtained on the Cu(100) surface. In the mean time, physisorption state of CH_3OH is also obtained on the Cu(111) surface. Although the chemical reduction in industry should be operated practically at elevated temperatures, the reaction free energies in Table 1 were calculated for room temperature (298K) so that the potential effect can be easily determined.

Although the chemical hydrogenation reactions of CO_2 to CH_3OH, CH_4 and C_2H_4, namely, $CO_2(g) + 3H_2(g) \rightarrow CH_3OH + H_2O$, $CO_2(g) + 4H_2(g) \rightarrow CH_4 + 2H_2O$ and $CO_2(g) + 3H_2(g) \rightarrow 1/2C_2H_4 + 2H_2O$, have rather negative overall reaction free energies of -109.45 kJ·mol^{-1}, -232.43 kJ·mol^{-1} and -180.46 kJ·mol^{-1}, respectively, some of the elementary reaction steps, especially the reaction steps of CO, have rather positive reaction free energies. This might be the reason why these reactions are practically difficult.

The DFT-calculated activation energies for H_2 dissociation are 0.52 eV and 0.45 eV, respectively on the Cu(111) and Cu(100) surfaces, which are relatively small as compared with the activation barriers for other steps in CO_2 reduction as shown later on. Therefore, the H_2 dissociation also should play a relatively minor role in the kinetics of the CO_2 chemical reduction by H_2.

In the following, we will first deduce the most possible pathways for the chemical reduction of CO_2 on the two types of Cu surfaces according to the calculated reaction free energies shown in Table 1 and the activation barriers determined from CI-NEB method. The mechanisms of the electrochemical reduction will be then discussed by analyzing the effect of electrode potentials on the steps in these pathways in the basis of the theoretical hydrogen electrode model, and by considering the water in the double layer as the hydrogenation agent in electrochemical environment.

Table 1 Possible reduction steps in chemical reduction of CO_2 and their reaction free energies on the Cu(111) and Cu(100) surface calculated with DFT.

Possible reaction steps	Reaction free energies, ΔG_{reac} (kJ mol^{-1})[a]	
	Cu(111)	Cu(100)
$1/2H_2(g)\rightarrow H^*$	-45.67	-41.34
(1a) $CO_2(g)+H^*\rightarrow HCOO^*$	-28.47	-50.66
(1b) $CO_2(g)+H^*\rightarrow COOH^*$	32.91	36.35
(1c) $CO_2(g)\rightarrow CO^*+O^*$	91.47	22.57
(1d) $COOH^*\rightarrow CO^*+OH^*$	-36.22	-49.87
(2a) $CO^*+1/2H_2(g)\rightarrow COH^*$	96.92	63.59
(2b) $CO^*+1/2H_2(g)\rightarrow CHO^*$	60.04	41.41
(2c) $CO^*\rightarrow OCCO^*$	132.55	75.59
(2d) $CO^*\rightarrow C^*+O^*$	263.66	154.73
(2e) $COH^*\rightarrow CHO^*$	-36.88	-22.18
(3a) $CHO^*+1/2H_2(g)\rightarrow CH_2O^*$	-40.49	-63.45
(3b) $COH^*+1/2H_2(g)\rightarrow CHOH^*$	-25.13	2.30
(3c) $COH^*\rightarrow C^*+OH^*$	78.26	5.38
(3d) $CHO^*\rightarrow CH^*+O^*$	67.59	27.82
(4a) $CH_2O^*+1/2H_2(g)\rightarrow CH_2OH^*$	-29.99	-1.64
(4b) $CH_2O^*+1/2H_2(g)\rightarrow CH_3O^*$	-127.37	-99.55
(4c) $CH_2O^*+1/2H_2(g)\rightarrow CH_2^*+OH^*$	-42.45	-47.05
(4d) $CH_2O^*\rightarrow CH_2^*+O^*$	41.87	10.11
(4e) $CHOH^*+1/2H_2(g)\rightarrow CH_2OH^*$	-82.22	-89.57
(4f) $CHOH^*\rightarrow CH_2O^*$	-52.23	-87.93

(4g) CHOH*→CH*+OH*	-22.44	-110.11
(5a) $CH_2OH^*+1/2H_2(g)\rightarrow CH_3OH$ (l)	-112.67	-96.53
(5b) $CH_2OH^*\rightarrow CH_2^*+OH^*$	-12.46	-45.41
(5c) $CH_3O^*+1/2H_2(g)\rightarrow CH_3OH$ (l)	-15.29	1.38
(5d) $CH_2OH^*\rightarrow CH_3O^*$	-97.38	-97.91
(5e) $CH_2OH^*+1/2H_2(g)\rightarrow CH_3^*+OH^*$	-118.31	-126.97
(5f) $CH_3O^*+1/2H_2(g)\rightarrow CH_3^*+OH^*$	-20.93	-29.07
(6a) $CH_2^*+1/2H_2(g)\rightarrow CH_3^*$	-105.85	-61.37
(6b) $CH_3^*+1/2H_2(g)\rightarrow CH_4(g)$	-99.41	-78.61
(6c) $CH_2^*\rightarrow 1/2C_2H_4^*$	-42.70	-92.59

The asterisk (*) indicates that the species is adsorbed on the surface

[a]In the calculations, the entropies obtained from the literature of Nørskov and coworkers[37, 38] are considered for gaseous molecules including CO_2, H_2, CH_3OH, CH_4 and C_2H_4, whereas the entropies of the adsorbed species are ignored. The zero point energies (*ZPE*) for all species, which are taken from the literature of Nørskov and coworkers,[37, 38] are included in the calculations. For steps involving the co-adsorption of two species, the co-adsorption structures was optimized and used in calculations. For instance, for reaction step of (A+B)* → (C+D)*, the reaction free energy is calculated according to "*E*(slab-C, D) − *E*(slab-A, B) + *ZPE*(C*) + *ZPE*(D*) − *ZPE*(A*) + *ZPE*(B*)".

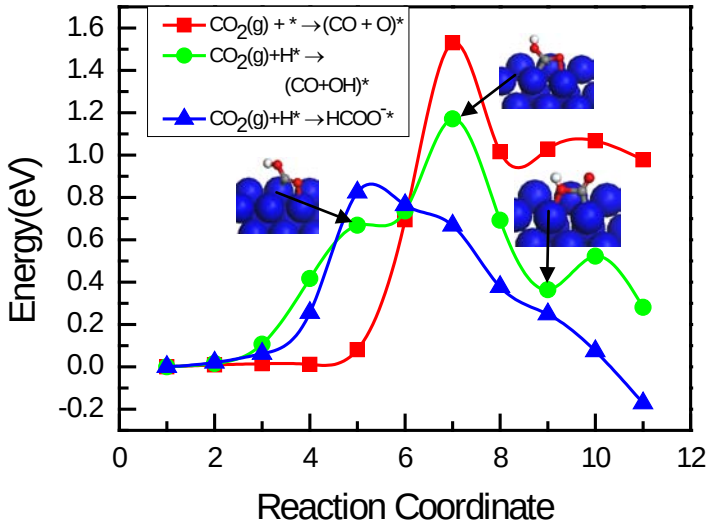

Fig. 1 Minimum energy paths for the three possible initial steps in the chemical reduction of CO_2 on the Cu(111) surface. Oxygen atoms are red, hydrogen atoms are white, carbon atoms are gray, and copper atoms are blue.

3.1.1 The first steps of CO_2 chemical reduction - Formation of CO

According to the calculated reaction free energies in Table 1, the direct dissociation of CO_2 into an adsorbed CO* and an adsorbed O* is the most endergonic process among various possible initial steps for the CO_2 chemical reduction on the Cu(111) surface, while the hydrogenation of CO_2 to an adsorbed formate (HCOO*) is the most exergonic process. In comparison, the hydrogenation to carboxyl (COOH) and the hydrogenative dissociation to the adsorbed CO and OH are both mild exergonic processes.

Fig. 1 displays the calculated MEPs for these possible initial steps on the Cu(111) surface. In these calculations, the initial state contains a physi-sorbed CO_2 molecule and a chemisorbed H* at the fcc site. The calculated activation energies for these steps follow the same trend as the reaction free energies. That is, the direct dissociation of CO_2 exhibits the highest activation barrier (~1.54 eV), while the formation of formate by direct hydrogenation of CO_2 requires the lowest activation energy (~0.86 eV). The activation barrier for the formation of carboxyl (COOH) is ca. 1.18 eV. The dissociative hydrogenation of CO_2 to adsorbed CO and OH is not an elementary step. It involves COOH as an intermediate, whose dissociation requires an activation energy of only ca. 0.2 eV. Thus, both the reaction free energies and activation energies from DFT calculations suggest that the formate is the most preferred initial product in the chemical reduction of CO_2 on the Cu(111) surface. The formation of CO from CO_2 is most probably through the COOH intermediate, which is formed with an activation barrier a bit higher than the formate formation. Experiment starting with formate showed no detectable products, and CO products was suppressed at a less negative potential when starting with CO_2.[20, 23]

Similar to that on the Cu(111) surface, the formation of formate is a relatively strong exergonic process (~92.00 kJ mol^{-1}). In comparison to that on the Cu(111) surface, however, the formation of COOH becomes much less exergonic while in the mean time the direct dissociation of the CO_2 becomes much less endergonic on the Cu(100) surface. If considering the hydrogenation may occur through adsorbed H atom, the reaction free energy for the formation of COOH could be more endergonic than the dissociation of CO_2. As will be shown in the later MEP calculations, the direct dissociation of CO_2 on the Cu(100) surface requires lower activation energy than its hydrogenation to COOH.

As shown in Fig. 2, the CO formation through the direct dissociation of CO_2 requires considerably lower activation energy (1.29 eV) than that through the hydrogenative dissociation (1.79 eV) on the Cu(100) surface, which is different from that on the Cu(111) surface. Therefore, direct dissociation of CO_2 would be the more preferred pathway for CO formation on the Cu(100) surface.

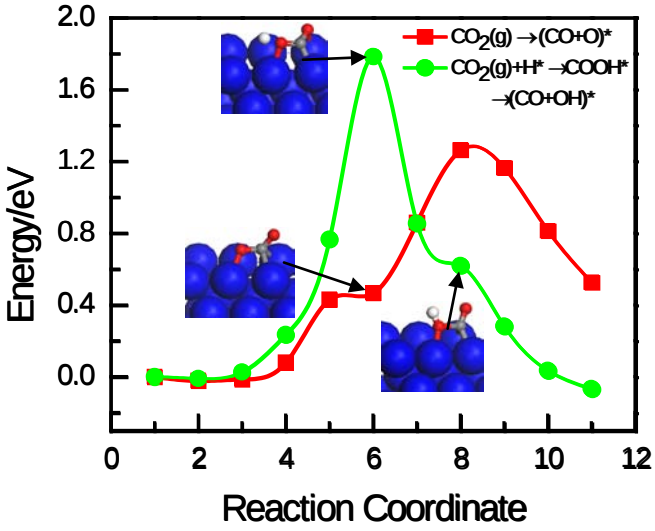

Fig. 2 Minimum energy path of CO formation on the Cu(100) surface from direct dissociation and hydrogenation of CO_2. Oxygen atoms are red, hydrogen atoms are white, carbon atoms are gray, and copper atoms are blue.

3.1.2 Reaction pathways of CO

There are three possible reactions for the formed CO, namely, the direct dissociation to adsorbed C* and O*, the hydrogenation to form an adsorbed formyl (CHO*), and the hydrogenation to form an adsorbed hydroxymethylidyne (COH*). Both the calculated reaction free energies (Table 1) and the MEPs (Fig. 3a) suggest that these reaction paths are endergonic, with the direct dissociation is particularly energetically demanding (2.75 eV and 3.96 eV respectively in reaction and activation free energies). Although the two hydrogenation reactions don't significantly differ from each other in reaction free energies (ca. 1.0 eV and 0.67 eV), the formation of CHO* requires an activation barrier nearly 1.5 eV lower than the formation COH* (~1.0 eV vs ~2.6 eV). On this basis, we may conclude that the most possible reaction path for CO is its hydrogenation to CHO*. By carefully inspecting the intermediate images in the calculated MEPs for the two hydrogenation reaction paths, one can find that the COH* formation actually involves CHO* as the intermediate.

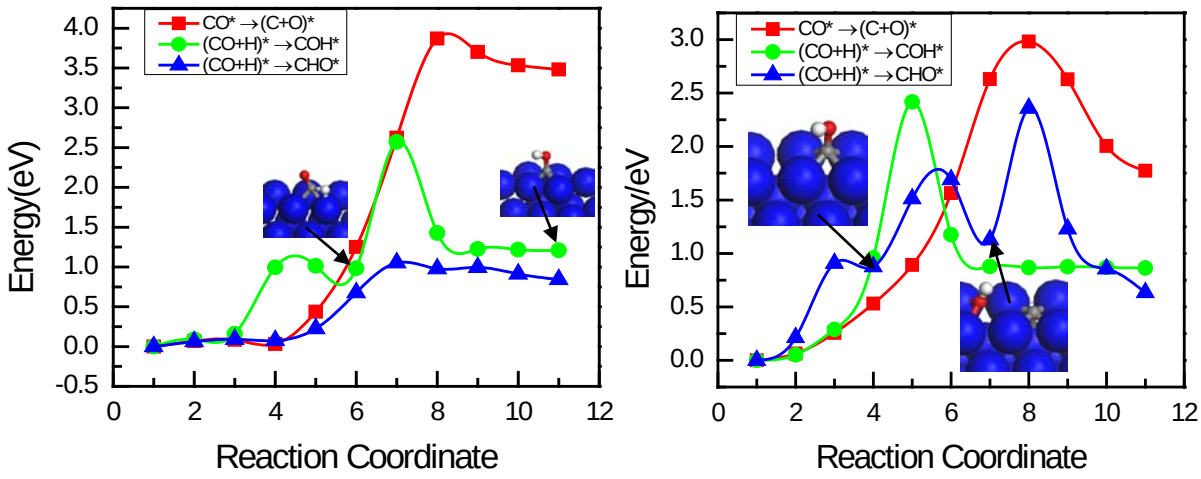

(a) (b)

Fig. 3 Minimum energy path of CO dissociation and hydrogenation to form C, COH and CHO (a) on the Cu(111) surface and (b) on the Cu(100) surface, respectively. Oxygen atoms are red, hydrogen atoms are white, carbon atoms are gray, and copper atoms are blue.

The calculated MEPs for the steps on the Cu(100) surface following the CO formation suggest they are very similar to that on the Cu(111) surface. The activation energy barriers for the direct dissociation, hydrogenation to form COH* and CHO* of CO required is 3.01, 2.43, and 2.36eV, respectively, as shown in Fig. 3b. These results indicated that CO hydrogenation requires higher activation energy barriers on the Cu(100) surface, which is more easily to achieve on the Cu(111) surface. By carefully inspecting the intermediate images in the calculated MEPs for the two hydrogenation reaction paths on the Cu(100) surface, one can find that the CHO* formation involves COH* and dissociative adsorption state C* + OH* as the intermediates.

In fact, the formation of formyl intermediate has been recognized in other reactions involving CO hydrogenation, for examples, alcohol production from carbon monoxide and molecular hydrogen on the Rh(111) surface,[39] Rh/TiO_2[40] and Rh/SiO_2 catalysts[41, 42], and formaldehyde and methanol synthesis from CO and H_2 on the Ni(111) surface.[43]

3.1.3 Reaction steps following CO hydrogenation

Among the three possible reaction paths of CHO*, the hydrogenation to the adsorbed formaldehyde (CH_2O*) is the most exergonic process in thermodynamics (-0.42 eV reaction free energy) and requires the lowest activation energy (ca. 0.7 eV). The other processes, including the hydrogenation to CHOH*, and the dissociation to CH*+O* and/or C*+OH*, require activation energies near or above 2.0 eV, as shown in Fig. 4, although the hydrogenation reaction to CHOH* is only a mild endergonic process in thermodynamics (0.12 eV reaction free energy). Therefore, the CH_2O* should be a key intermediate after CHO* formation for

the CO_2 chemical reduction on the Cu(111) surface.

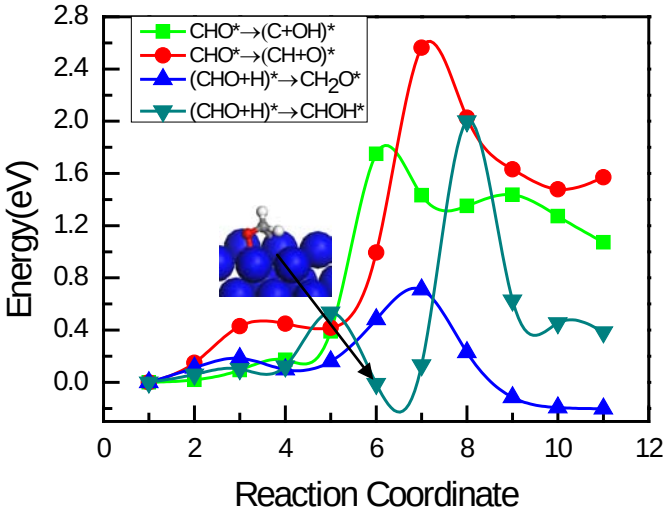

Fig. 4 Minimum energy path of on the Cu(111) surface CHO dissociation and hydrogenation into CH, C, CHOH and CH_2O, respectively. Oxygen atoms are red, hydrogen atoms are white, carbon atoms are gray, and copper atoms are blue.

In a previous study on the mechanism of ethanol synthesis from syngas on the Rh(111) surface, Liu *et al.*[39] showed that the CHO* intermediate formed through CO hydrogenation can be more easily hydrogenated to form CH_2O* than the dissociation. Earlier studies[13, 23] also have shown that CH_4 can be synthesized on Cu with formaldehyde (CH_2O) as the starting material.

The CH_2O may undergo direct dissociation to methylene ($:CH_2$) and O*, direct hydrogenation to form CH_3O* and/or CH_2OH, and/or hydrogenated dissociation to methylene ($:CH_2$) and OH. The calculated reaction free energies for the formation of the CH_3O* or and/or CH_2OH* are -127.37 kJ mol^{-1} and -29.99 kJ mol^{-1}, respectively, while it is -49.08 kJ mol^{-1} for the $:CH_2$ formation. This seems to suggest that the CH_3O* pathway is preferable on the Cu(111) surface. As shown by the MEP calculation results in Fig. 5, the formation of CH_3O* and the hydrogenated dissociation of CH_2O* to $:CH_2$ actually proceed via CH_2OH* intermediate, which has lower activation energy than the CH_2O* direct dissociation. Therefore, although the reaction free energy of the CH_2OH* formation is less exergonic than CH_3O*, the preferred reaction pathway of the CH_2O* should be the hydrogenation to form CH_2OH* rather than CH_3O*.

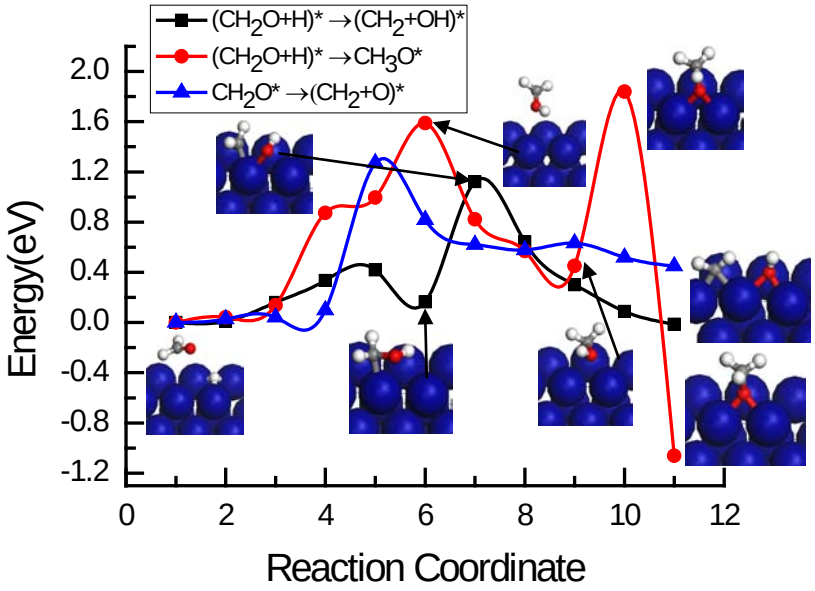

Fig. 5 Minimum energy paths of the direct hydrogenation, the hydrogenative dissociation, and direct dissociation of CH_2O on the Cu(111) surface, respectively. Oxygen atoms are red, hydrogen atoms are white, carbon atoms are gray, and copper atoms are blue.

It can be seen that the formation of CH_2 and OH via CH_2O* hydrogenative dissociation is not an element step in Fig. 5. The hydrogenation of CH_2O* first produces CH_2OH* intermediate with an activation barrier of about 0.48 eV, the transformation of CH_2OH* to CH_2 and OH requires the activation barrier of about 1.04 eV. As shown by the calculated MEPs in Fig. 6, the activation barriers for the direct hydrogenation of CH_2OH* to form CH_3OH and the hydrogenative dissociation of CH_2OH* to form CH_2 are ~0.68 eV, and 0.66 eV, respectively. Thus, CH_2OH* intermediate either forms CH_3OH by direct hydrogenation or forms CH_2 by hydrogenative dissociation. Based on the activation barriers, the simultaneous occurrence of both paths can be concluded, which maybe a parallel path in CO_2 reduction mechanism on the Cu(111) surface. Additionally, the hydrogenative reduction of CH_2OH* to CH_3OH and the hydrogenative dissociation to form CH_2 and H_2O is also easier than the abovementioned CH_2OH direct dissociation. The results presented explained the experiment results in which CH_3OH was observed in CO_2 chemical reduction on copper surfaces.

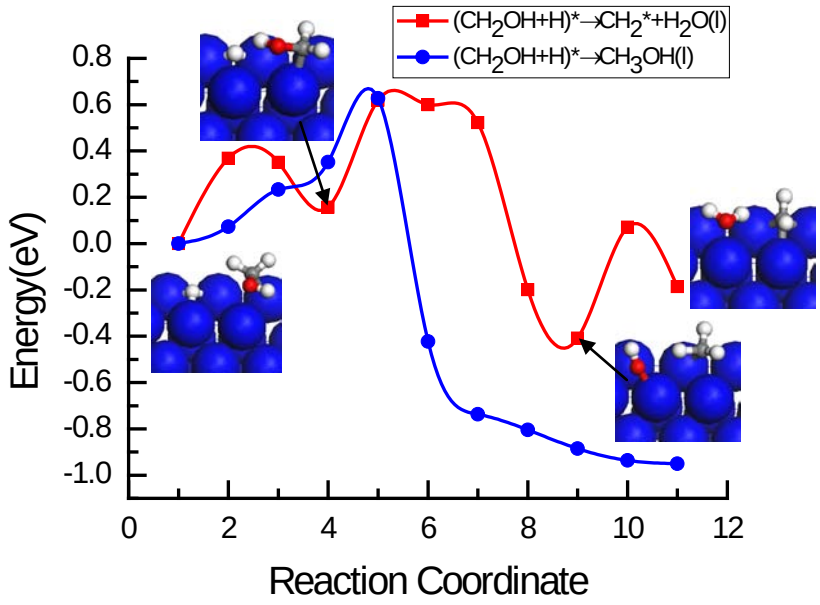

Fig. 6 Minimum energy paths of the direct hydrogenation to CH_3OH, and the hydrogenative dissociation to CH_2 and H_2O of CH_2OH on the Cu(111) surface, respectively. Oxygen atoms are red, hydrogen atoms are white, carbon atoms are gray, and copper atoms are blue.

The formation of CH_4 through CH_2 hydrogenation is drastically exergonic on the Cu(111) surface. In comparison, the C_2H_4 formation is less exergonic. This explains the experimental results that CH_4 is more likely formed on the Cu(111) surface. Fig. 7a shows the MEPs for the formation of CH_4 and C_2H_4 from CH_2. The activation barriers for the two hydrogenation steps in CH_4 formation are 0.63 eV and 1.03 eV, respectively. For the association of two CH_2 to C_2H_4, the activation barrier is 0.21eV, which is less than that of CH_2 hydrogenation to CH_3. This seemingly indicated that CH_2 dimerization to C_2H_4 is kinetically more favorable. However, as shown by the calculated MEPs in Fig. 6, CH_3 and OH intermediate is observed during the course of CH_2OH hydrogenative dissociation to CH_2 and H_2O, and the reaction free energy of forming CH_3 and OH intermediate is more negative than that of forming CH_2 and H_2O, an activation barriers of ~0.53 eV is required from CH_3 and OH to CH_2 and H_2O, namely, CH_3 intermediate maybe easier to form on the Cu(111) surface, considering that the surface coverage of the CH_2 should be very low, the dimerization reaction thus would still have much lower reaction rate than the hydrogenation reaction on the Cu(111) surface.

However, on the Cu(100) surface, we find that the CH_2 dimerization into C_2H_4 is a nonactivated process, as shown in Figure 7b. The paths for CH_3 and CH_4 formation require activation energy barriers of 0.34 and 0.55eV, respectively. The dimerization of CH_2 to C_2H_4 has more negative reaction free energy than that of CH_2 hydrogenation to CH_3. Thus, C_2H_4 formation should be more easily on the Cu(100) surface than the CH_4 formation.

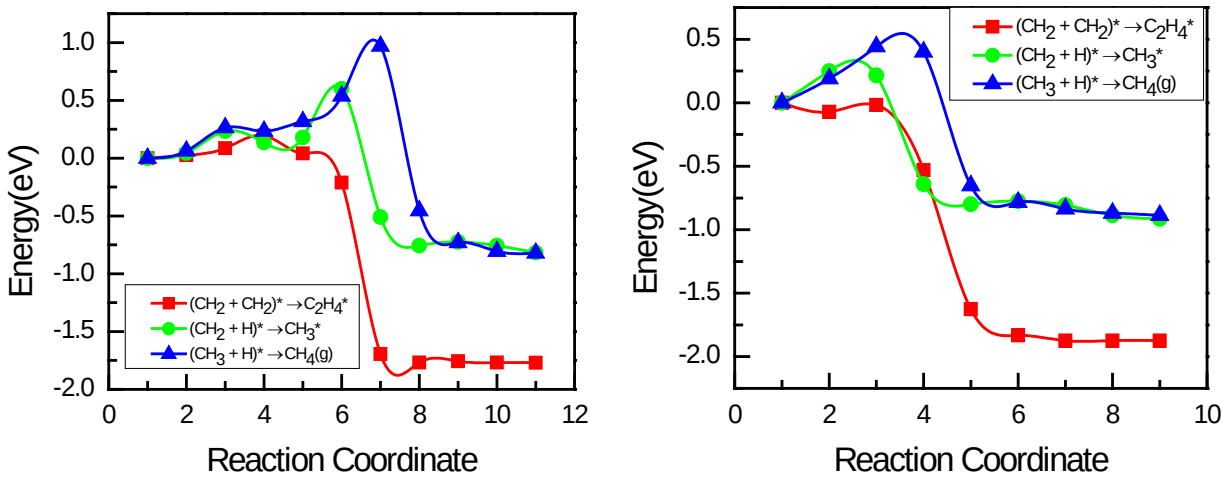

Fig. 7 Minimum energy paths of CH_2 successive hydrogenation into hydrocarbons CH_3, CH_4 and dimerization into C_2H_4 (a) on the Cu(111) surface and (b) on the Cu(100) surface, respectively.

The results from Koper and coworkers[21] suggested that there are two separate pathways for the formation of C_2H_4, one that shares an intermediate with the pathway to CH_4, as we observed on the Cu(111) surface and below −0.8 V on the Cu(100) surface at pH 7, and a second pathway that occurs only on the Cu(100) surface. For this second pathway, we suggest that the formation of a CO dimer is the key intermediate in the formation of C_2H_4. As shown in Figure 8, the activation energy barriers for the formation of CO dimer on the Cu(111) and Cu(100) surface are 1.59 and 1.26 eV, respectively. The results indicated that CO dimerization requires higher activation energy barrier than CO hydrogenation to form CHO* on the Cu(111) surface, whereas on the Cu(100) surface, which requires lower activation energy barrier than CO hydrogenation to form CHO*. Therefore, CO hydrogenation is more easily to occur on the Cu(111) surface, whereas CO dimerization into $(CO)_2$ is more easily to achieve on the Cu(100) surface. Such a surface dimer could explain the unique selectivity for C_2H_4 (for detailed arguments, see ref 7) and is in agreement with the suggestion of Gatrell et al[8] who proposed that this CO dimer would be more stable on the Cu(100) surfaces. Additionally, our results may somewhat agree with Koper and coworkers.

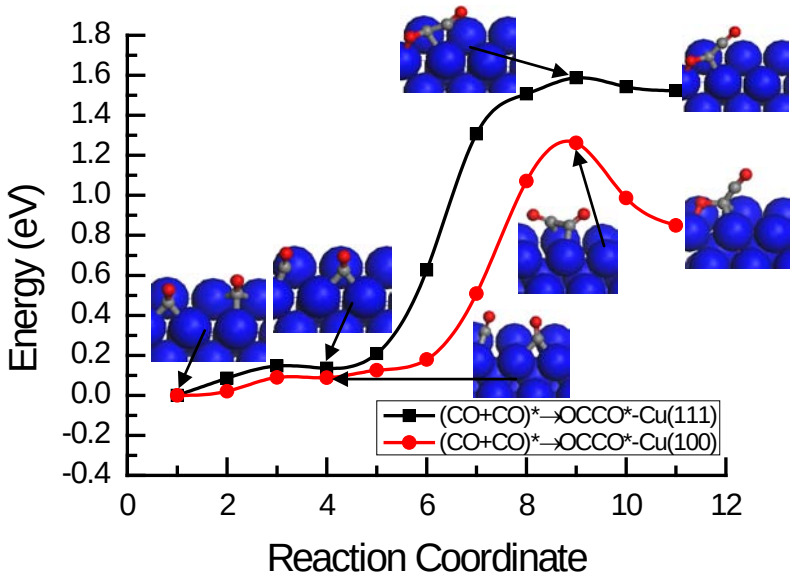

Fig. 8 Minimum energy paths of CO dimerization into OCCO* on the Cu(111) and Cu(100) surfaces.

Based on above reaction free energy and MEP calculation results, the optimal reaction paths for CO_2 reduction to hydrocarbons on the Cu(111) surface can be summarized in Table 2. CO is firstly formed by dissociative hydrogenation of CO_2, the most possible reaction path for CO is its hydrogenation to CHO* intermediate, the key intermediate CH_2O can be more easily formed through CHO further hydrogenation, the preferred reaction pathway of the CH_2O should be the hydrogenation to form CH_2OH, based on the activation energy barriers, the CH_2OH intermediate either forms CH_3OH by direct hydrogenation or forms CH_2 by hydrogenative dissociation, which maybe a parallel path in CO_2 reduction mechanism on the Cu(111) surface, finally, the CH_2 intermediate lead to formation of the hydrocarbons. From kinetic view of point, the relatively slow steps on the Cu(111) surface include $CO_2(g) + H^* \rightarrow (CO + OH)^*$, $(CO + H)^* \rightarrow CHO^*$. The reason may be that the weak Cu-CO_2 interaction is an obstacle to CO_2 dissociative hydrogenation and therefore slows down the overall conversion. The differences in the reaction mechanism on the Cu(111) and Cu(100) surfaces are that the CO formation and further reduction undergoes different pathway. Simultaneously, the preference in the formation of CH_4 and C_2H_4 is also different, the formation of C_2H_4 is easier on the Cu(100) surface, and the experimental results are explained to some degree on the selectivity of Cu single crystal surface. The C_2H_4 formation mechanisms via CO dimerization will be studied systematically in our future work.

Table 2 The minimum energy paths for the chemical reduction of CO_2 to hydrocarbons and the activation energy barriers (E_{act}) in each elementary step on the Cu(111) surface.

Reaction Paths	E_{act} (eV)

$CO_2(g) + * \rightarrow (CO + O)*$	1.54 (1.29)[a]
$CO_2(g) + H* \rightarrow (CO + OH)*$	1.18 (1.79)
$(CO + H)* \rightarrow CHO*$	1.06
$(CHO + H)* \rightarrow CH_2O*$	0.72
$(CH_2O + H)* \rightarrow (CH_2 + OH)*$	1.12
$(CH_2O + H)* \rightarrow CH_2OH*$	0.95
$(CH_2O + H)* \rightarrow CH_3O*$	1.86
$(CH_2OH + H)* \rightarrow CH_3OH$ (l)	0.68
$(CH_2OH + H)* \rightarrow CH_2* + H_2O$ (l)	0.66
$(CH_2 + H)* \rightarrow CH_3*$	0.63 (0.34)
$(CH_3 + H)* \rightarrow CH_4$ (g)	1.03 (0.56)
$2CH_2* \rightarrow C_2H_4*$	0.21 (~0)

[a]The values in parentheses are the activation energy barriers of corresponding processes on the Cu(100) surface.

3.2 Electrochemical reduction of CO_2

One of the major differences between the electrochemical reduction and the chemical reduction is that the H_2 molecules will be replaced by the $(H^+ + e)$ pair. The overall reaction for electrochemical reduction of CO_2 to methanol and hydrocarbons can be expressed as follows,

$$CO_2(g) + 8(H^+ + e^-) \rightarrow CH_4 + 2H_2O \quad (2a)$$

$$CO_2(g) + 6(H^+ + e^-) \rightarrow 1/2C_2H_4 + 2H_2O \quad (2b)$$

$$CO_2(g) + 6(H^+ + e^-) \rightarrow CH_3OH + H_2O \quad (2c)$$

Since that the chemical potential (μ) of electron changes with the electrode potential (E), the reaction free energies would vary with E. If the potential of the reversible hydrogen electrode (RHE) is used as the zero potential, one would have $\mu(H^+ + e^-) = 1/2\mu(H_2) - eE$.[44] This relation provides an elegant way to calculate the potential-dependent free energies of the reaction steps in the electrochemical reduction by avoiding the explicit treatment of solvated protons.

In electrochemical reduction, the reaction steps involving hydrogenation will be enhanced thermodynamically as potential goes negative. In addition, for reaction steps which produce O* or OH*, the reaction may be promoted since these oxygenated species can be easily removed from the surface at negative potentials. Experimental results[9, 16, 20] have shown that when electrode potential is -0.50 V (*vs*. RHE), formate is main product, when electrode potential is -0.67 V (*vs*. RHE), CO is main product, when electrode potential is more negative, that is -0.90 V (*vs*. RHE), hydrocarbons start to form. We chose the three mentioned

electrode potential to calculate the reaction free energies for various steps and the results are given in Table 3.

The free energies ΔG_{reac} on the Cu(111) surface for the overall reactions 2a are -618.43 kJ mol^{-1}, -749.67 kJ mol^{-1}, and -927.23 kJ mol^{-1}, the ΔG_{reac} are -469.96 kJ mol^{-1}, -568.39 kJ mol^{-1}, and -701.56 kJ mol^{-1} for the overall reactions 2b, and the ΔG_{reac} are -389.95 kJ mol^{-1}, -497.38 kJ mol^{-1}, and -630.55 kJ mol^{-1} for the overall reactions 2c when the electrode potential is -0.50 V, -0.67 V, and -0.90 V (*vs*. RHE), respectively, which are all highly exergonic. The ΔG_{reac} under electrochemical environment is more negative than that in chemical reduction. Therefore, these reactions may be more favorable under electrochemical environment.

Table 3 Possible reduction steps in electrochemical reduction of CO_2 to Hydrocarbon and their reaction free energies on the Cu Surface calculated with DFT

Possible Reduction steps	Reaction free energies, ΔG_{reac} (kJ mol^{-1})					
	Cu(111)			Cu(100)		
	-0.50 V	-0.67	-0.90	-0.50 V	-0.67	-0.90
(a) $CO_2(g) + H^+ + e^- \rightarrow HCOO^*$	-98.06	-114.47	-136.66	-119.84	-136.25	-158.44
(b) $CO_2(g) + H^+ + e^- \rightarrow COOH^*$	-16.29	-32.70	-54.89	-32.83	-49.24	-71.43
(c) $COOH^* + H^+ + e^- \rightarrow CO^* + H_2O$ (l)	-84.07	-101.48	-123.67	-73.12	-89.53	-111.72
(d) $HCOO^* + H^+ + e^- \rightarrow CO^* + H_2O$ (l)	-3.30	-19.71	-41.90	13.89	-2.52	-24.71
(e) $CO^* + H^+ + e^- \rightarrow CHO^*$	11.79	-4.62	-26.81	-6.84	-23.25	-45.44
(f) $CO^* + H^+ + e^- \rightarrow COH^*$	48.67	32.26	10.07	15.34	-1.07	-23.26
(g) $CHO^* + H^+ + e^- \rightarrow C^* + H_2O$ (l)	84.63	68.22	46.03	-25.48	-41.89	-64.08
(h) $CHO^* + H^+ + e^- \rightarrow CH^* + OH^*$	-58.95	-75.36	-97.55	-133.88	-150.29	-172.48
(i) $CH^* + OH^* + H^+ + e^- \rightarrow CH^* + H_2O$ (l)	-48.84	-65.25	-87.44	-23.25	-39.66	-61.85
(j) $CHO^* + H^+ + e^- \rightarrow CH_2O^*$	-88.74	-105.15	-127.34	-111.70	-128.11	-150.30
(k) $CHO^* + H^+ + e^- \rightarrow CHOH^*$	-36.50	-52.91	-75.10	-23.77	-40.18	-62.37
(l) $CH_2O^* + H^+ + e^- \rightarrow CH_3O^*$	-175.62	-192.03	-214.22	-147.80	-164.21	-186.40
(m) $CH_2O^* + H^+ + e^- \rightarrow CH_2OH^*$	-78.24	-94.65	-116.84	-49.89	-66.30	-88.49
(n) $CH_2OH^* + H^+ + e^- \rightarrow CH_3OH$ (l)	-160.92	-177.33	-199.52	-144.78	-161.19	-183.38
(o) $CH_3O^* + H^+ + e^- \rightarrow CH_3OH$ (l)	-63.54	-79.95	-102.14	-46.87	-63.28	-85.47
(p) $CH_2O^* + H^+ + e^- \rightarrow CH_2^* + OH^*$	-90.71	-107.12	-129.31	-95.30	-111.71	-133.9
(q) $CH_2^* + OH^* + H^+ + e^- \rightarrow CH_2^* + H_2O$ (l)	-48.84	-65.25	-87.44	-23.25	-39.66	-61.85

(r) $CH_2^* + H^+ + e^- \rightarrow CH_3^*$	-154.10	-170.51	-192.70	-129.82	-146.23	-168.42
(s) $CH_3^* + H^+ + e^- \rightarrow CH_4$ (g)	-147.66	-164.07	-186.26	-146.09	-162.50	-184.69
(t) $CH_2^* \rightarrow 1/2C_2H_4^*$	-85.40	-85.40	-85.40	-185.18	-185.18	-185.18

According to the calculated electrochemical reaction free energies, the formation of formate and COOH will be both promoted at negative electrode potentials. In electrochemical condition, the hydrogenated dissociation of COOH to CO would become a favorable step as potential goes more negative than -0.67 V. The subsequent protonation of CO also gradually becomes highly exergonic. Therefore, the hydrocarbons would become the favored products in the electrochemical reduction, especially at more negative potentials. These results are in accordance with experimental results.[9, 16, 20]

Under the electrochemical condition, CHO* could undergo a hydrogenated dissociation to CH due to that the OH and O can be easily removed from the surface. As potential is more negative than -0.67 V, the formation of CH could become more favored than the formation of CH_2O^*. However, as shown in Fig. 4, activation energy for CHO hydrogenation to form CH_2O^* is ca. 0.7 eV, the dissociation to CH*+O* require activation energies above 2.0 eV. CH_2O^* could undergo a hydrogenated dissociation to $CH_2^* + H_2O$ or hydrogenated directly to CH_3O^* or CH_2OH^*. As potential is more negative than -0.90 V, the formation of $CH_2^* + H_2O$ and CH_3O^* are strong exergonic processes, and free energies ΔG_{reac} are approximately equal, indicating that $CH_2^* + H_2O$ and CH_3O^* may be formed simultaneously by CH_2O^* further reduction. However, as shown in Fig. 6, CH_3O^* formation requires a higher activation energy. Thus, the formation of $CH_2^* + H_2O$ could become more favored. It is worth considering why CH_3OH is formed in gas phase chemistry[45] and CH_4 is formed in electrochemistry[16, 17] on copper surfaces. In the current study, we considered that adsorbed CH_3O^* or CH_2OH^* may form CH_3OH via a proton-transfer reaction. However, our calculations showed that the free energies ΔG_{reac} of CH_2OH^* formation is more positive than CH_2O^* hydrogenate dissociation to $CH_2^* + H_2O$, and CH_3O^* formation requires a higher activation energy, this would be in favor of CH_4 formation, in agreement with the electrochemical experiment results in which only CH_4, and not CH_3OH, was observed. Accordingly, we speculate that the optimum electrochemical reduction path of CO_2 on the Cu(111) surfaces are $CO_2(g) + 2(H^+ + e^-) \rightarrow CO^* + H_2O$, $CO^* + (H^+ + e^-) \rightarrow CHO^*$, $CHO^* + (H^+ + e^-) \rightarrow CH_2O^*$, $CH_2O^* + 2(H^+ + e^-) \rightarrow CH_2^* + H_2O$, $CH_2^* + (H^+ + e^-) \rightarrow CH_3^*$, $CH_3^* + (H^+ + e^-) \rightarrow CH_4(g)$, in which $CO^* + (H^+ + e^-) \rightarrow CHO^*$ may be potential-limiting step. Similar conclusion has been obtained by Nørskov and coworkers.[37]

In the calculations conducted by Nørskov *et al.*,[37, 38] the direct hydrogenation was considered as the

major reaction of CH_2O*. Therefore, the key intermediate for the formation of hydrocarbons in their reaction mechanism is CH_3O*. By comparing the calculated reaction free energies and activation energies for the two pathways, we can find that the hydrogenated dissociation pathway is actually more favorable. Koper *et al.*[46, 47] have reported their studies of the reduction of CO_2 on two basal planes, Cu(111) and Cu(100), using online electrochemical mass spectrometry (OLEMS) to investigate the path to CH_4 and C_2H_4. This tip-based sampling technique allows the formation of volatile reaction intermediates and products to be followed while the potential at the electrode is changed. One can measure the reduction of the various species online while changing the potential and, therefore, follow the formation and consumption of intermediates during the reaction. Their experimental results show that it is very likely that CHO_{ads} is the key intermediate towards the breaking of the C-O bond and, therefore, the formation of CH_2, CH_3 species, and CH_4. CH_3O cannot be reduced to CH_4 on the copper electrodes. The experimental observations appears in conflict with the DFT calculated results from Nørskov *et al*., in which the DFT calculated results also suggest that CHO_{ads} is the intermediate in the formation of methane, however, the energetically favored route to CH_4 is through adsorbed CH_3O species.

In addition, it has been proposed in earlier studies that[48] the electrocatalytic reduction of CO_2 on Cu electrodes involves an initial stage forming the carbon dioxide anion radical $CO_2^{\cdot-}$, which is not observed on the Cu(111) surface in our previous calculations since the chemisorption state of CO_2 molecule is not obtained on the Cu(111) surface during the geometry optimization and minimum energy path analysis. Although the chemisorption state of CO_2 molecule is obtained on the Cu(100) surface, the adsorption energies of the chemisorption states of CO_2 molecule is positive, which indicated that the chemisorption state is metastable state. Indeed, in electrochemical reduction of CO_2, formate and COOH species are usually formed through anion radical $^{\cdot}CO_2^{-}$ protonation. Due to a large reorganizational energy between the linear molecule and bent radical anion, the outer-sphere single electron reduction of CO_2 to carbon dioxide anion radical should be difficult in both kinetics and thermodynamics.[1] However, when electrode potential is more negative, the electron level of electrode could be aligned with the LOMO of CO_2, electron transfer to CO_2 molecular is possible. If a proton transfer occurs simultaneously, the products could be more stable. This phenomenon can be verified by geometry optimization of CO_2 molecule in the presence of hydronium ion. Accordingly, in this section, we used hydronium ion $H_3O^+\cdots(H_2O)_3$ as model of solvation in acid solution in order to model the first proton-coupled electron transfer step during CO_2 reduction at Cu/electrolyte interface and evaluate the role of proton, in which the rationalization of model have been validated in our previous work.[49] Fig. 9 gives geometry structural optimization plot of the protonation of CO_2 in the presence of

hydronium ion $H_3O^+\cdots(H_2O)_3$. Optimized results indicated that anion radical $^{\cdot}CO_2^-$ is formed primarily, and then hydrated proton $H_9O_4^+$ preferentially combined with O atom in chemisorbed to form COOH species (Fig. 9a, b) other than formate species when CO_2 molecule adsorbed on the Cu(111) and Cu(100) surfaces for the protonation process, even if the hydrated proton $H_9O_4^+$ was closer to the C atom in the initial structure, namely, formate species formation may require higher activation energy than COOH under electrochemical environment. Based on the geometry optimization, it can be concluded that anion radical $^{\cdot}CO_2^-$ is formed primarily under electrochemical conditions, and then successive proton and electron transfer occur, eventually leading to the formation of hydrocarbons. Meanwhile, the experimental result[50] also indicated that the adsorption of alkali metal on the Cu surfaces promoted formation of carbon dioxide anion radical $^{\cdot}CO_2^-$. Thus, the reaction in experiment may be also promoted by alkali metal halides.

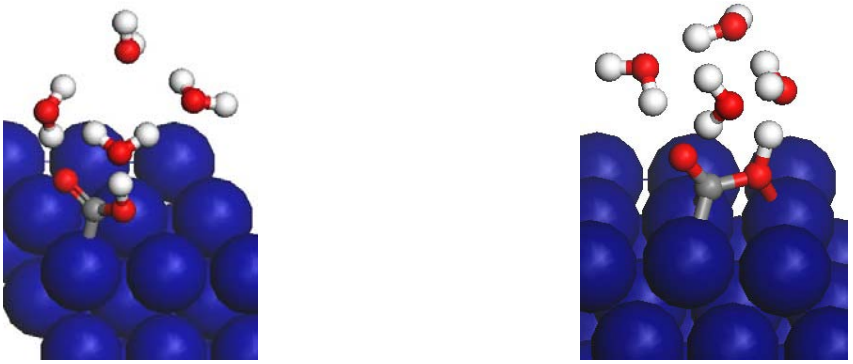

(a) (b)

Fig. 9 Geometry optimization plot of the protonation of CO_2 in the presence of hydrated proton $H_9O_4^+$: (a) COOH adsorbed on the Cu(111) surface and (b) COOH adsorbed on the Cu(100) surface.

Simultaneously, the above DFT calculations have also shown that there are two possibilities for hydrocarbons formation: One is chemical reduction through direct hydrogenation, via adsorbed hydrogen, which occurs by a surface chemistry reaction, for example:

$$(CH_2 + H)^* \rightarrow CH_3^*, \quad (CH_3 + H)^* \rightarrow CH_4(g)$$

Another possibility to produce hydrocarbons is direct electrochemical reaction:

$$CH_2^* + H^+ + e^- \rightarrow CH_3^*, \quad CH_3^* + H^+ + e^- \rightarrow CH_4(g)$$

The two routes are compared in Fig. 10 for Cu(111) surface at -0.90 V (*vs.* RHE). As can be seen, in the direct electrochemical route, it can be observed that the intermediate CH_2 formation is exergonic. CH_2 formation can be seen to be uphill in energy, and the free energies of CH_2 hydrogenation to form CH_4 are more positive in the hydrogenation route than that of the direct electrochemical route. Thus, the direct electrochemical route would be expected to be highly favored at potentials of interest to CO_2 reduction. Simultaneously, under electrochemical conditions, the free energy of CH_4 formation via two protonation

steps of CH_2 is more negative on the Cu(111) surface than that on the Cu(100) surface (as shown in Fig. 10), and the free energy of C_2H_4 formation is more negative than that of CH_2 protonation to form CH_3 on the Cu(100) surface (as shown in Table 3). Thus, DFT study indicated that CH_4 is favorably formed on the Cu(111) surface and C_2H_4 is preferably formed on the Cu(100) surface under electrochemical conditions, and the experimental results are explained.

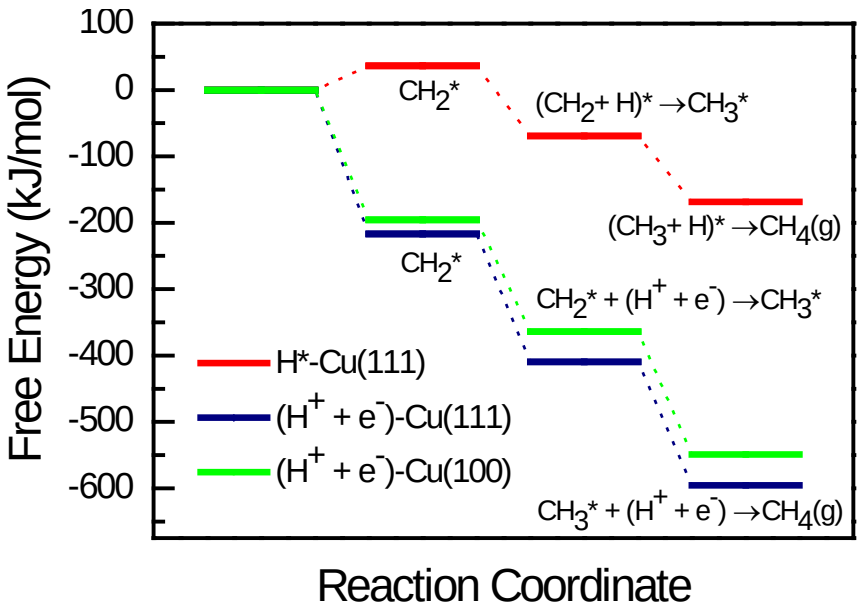

Fig. 10 Comparison of the production of CH_4(g) from CH_2* via the direct electrochemical route and the combination of adsorbed CH_2* and adsorbed H* on the Cu(111) surface, and effect of crystal face on selectivity of product.

The possible optimized reaction paths of CO_2 reduction to form hydrocarbons on Cu single crystal electrode surfaces and degree of difficulty of the reaction have been revealed, and systematical understanding of CO_2 reduction mechanism have also been achieved using density functional theory (DFT) method in the first principle on the geometry structural optimization, the reaction energies calculations and the minimum energy paths analysis. On this basis, the effect of alloying on activation barriers of rate-determining step and the reaction pathways into C_2H_4 via CO dimerization on the Cu (100) surface will be studied in the future. The research results have great significance for understanding in depth the selectivity of CO_2 electrochemical reduction process, the sensitivity of surface structure and size effect of catalysts. Simultaneously, the research results can provide a scientific basis for designing the catalysts of CO_2 electrochemical reduction.

5. Conclusions

A complete thermodynamic and kinetic description of CO_2 reduction on the Cu single crystal surfaces

is carried out for the first time based on a systematic DFT calculation exploration in this present work. New insight has been provided on the chemical and electrochemical reduction of CO_2 into hydrocarbons CH_4 at the atomic level on the Cu surfaces.

In agreement with the present experiment and theoretical studies, our DFT calculated results indicated that the CHO_{ads} and CH_2OH_{ads} is the key intermediate towards the chemical and electrochemical reduction of CO_2 into hydrocarbons, and CO dimerization is more easily to achieve, CO hydrogenation is difficult to occur on the Cu(100) surface, explaining the unique selectivity for C_2H_4. However, our DFT calculated results indicated CH_3O cannot be reduced to CH_4 on the copper electrodes, the main reaction of the CHO_{ads} is the hydrogenated dissociation to $:CH_2$, eventually leading to the formation of CH_3 species, and CH_4, which are consistent with the present experimental results, but conflicting with the present theoretical results. Additionally, DFT calculated results showed for the first time that the electrochemical reduction would be expected to be highly favored at potentials of interest to CO_2 reduction compared with the chemical reduction and the carbon dioxide anion radical ($\cdot CO_2^-$) is involved in the initial stage of CO_2 electroreduction.

By analyzing the chemical reduction pathways, we deduced important mechanistic information. The possible optimal pathway on the Cu(111) surface are $CO_2(g) + H^* \rightarrow COOH^* \rightarrow CO^* + OH^*$, $CO^* + H^* \rightarrow CHO^*$, $CHO^* + H^* \rightarrow CH_2O^*$ $CH_2O^* + H^* \rightarrow CH_2OH^* \rightarrow CH_2^* + OH^*$, $CH_2^* + H^* \rightarrow CH_3^*$, $CH_3^* + H^* \rightarrow CH_4(g)$. CO is firstly formed by dissociative hydrogenation of CO_2, the most possible reaction path for CO is its hydrogenation to CHO* intermediate, the key intermediate CH_2O can be more easily formed through CHO further hydrogenation, the preferred reaction pathway of the CH_2O should be the hydrogenation to form CH_2OH, based on the activation barriers, the CH_2OH intermediate either forms CH_3OH by direct hydrogenation or forms CH_2 by hydrogenative dissociation, which maybe a parallel path in CO_2 reduction mechanism on the Cu(111) surface, finally, the CH_2 intermediate lead to formation of the hydrocarbons. From kinetic view of point, the relatively slow steps on the Cu(111) surface include $CO_2(g) + H^* \rightarrow (CO + OH)^*$, $(CO + H)^* \rightarrow CHO^*$. The reason may be that the weak Cu-CO_2 interaction is an obstacle to CO_2 dissociative hydrogenation and therefore slows down the overall conversion. The differences in the reaction mechanism on the Cu(111) and Cu(100) surfaces are that the CO formation and further reduction undergoes different pathway. Simultaneously, the preference in the formation of CH_4 and C_2H_4 is also different, the formation of C_2H_4 is easier on the Cu(100) surface, and the experimental results are explained to some degree on the selectivity of Cu single crystal surface.

The free energies for various steps in the electrochemical reduction of CO_2 were calculated under

different electrode potentials. The results indicated that formate and CO are mainly formed when the potential is more positive than -0.50 V (*vs.* RHE). The protonated dissociation of CO_2 to form CO and the subsequent protonation of CO become increasingly exergonic as the potential goes negative, so that hydrocarbons gradually becomes the favored products during the electrochemical reduction. Under electrochemical conditions, the possible optimum reaction path on the Cu(111) surface are $CO_2(g) + 2(H^+ + e^-) \rightarrow CO^* + H_2O$, $CO^* + (H^+ + e^-) \rightarrow CHO^*$, $CHO^* + (H^+ + e^-) \rightarrow CH_2O^*$, $CH_2O^* + 2(H^+ + e^-) \rightarrow CH_2^* + H_2O$, $CH_2^* + (H^+ + e^-) \rightarrow CH_3^*$, $CH_3^* + (H^+ + e^-) \rightarrow CH_4(g)$, in which $CO^* + (H^+ + e^-) \rightarrow CHO^*$ may be potential-limiting step. Simultaneously, the calculated results also explained partly why CH_3OH is formed in gas phase chemistry and only CH_4 is observed in electrochemistry on copper surfaces.

Acknowledgements

This work is financially supported by the National Natural Science Foundation of China (Grant No. 21303048), Hunan Provincial Natural Science Foundation of China (Grant No. 13JJ4101), the Construct Program of the Key Discipline in Hunan Province (Applied Chemistry) and Doctoral Start-up Fund of Hunan University of Arts and Science.

References

1 F. Hasegawa, S. H. Yokoyama and K. Imou, *Bioresource Techno*., 2010, **101**, S109−S111.

2 M. Abu-zahra, L. H. Schneiders, J. P. M. Niederer, P. H. Feron and G. F. Versteeg, *Int. J. Greenh. Gas con*., 2007, **1**, 37−46.

3 B. P. Sullivan, *Electrochemical and Electrocatalytic Reduction of Carbon Dioxide*, Elsevier, Amsterdam, 1993.

4 C. M. Sanchez-Sanchez, V. Montiel, D. A. Tryk, A. Aldaz and A. Fujishima, *Pure Appl. Chem*., 2001, **73**, 1917−1927.

5 M. M. Halmann, *Greenhouse Gas Carbon Dioxide Mitigation*, Lewis Publishers, Washington, DC, 1999.

6 T. Inui, M. Anp, K. Izui, S. Yanagida, and T. Yamaguchi, *Advances in Chemical Conversions for Mitigating Carbon Dioxide*, Elsevier, Amsterdam, 1998.

7 Y. Hori, K. Kikuchi, A. Murata and S. Suzuki, *Chem. Lett*., 1986, **15**, 897−898.

8 Y. Hori, A. Murata, R. Takahashi and S. Suzuki, *J. Am. Chem. Soc*., 1987, **109**, 5022−5023.

9 J. J. Kim, D. P. Summers and K. W. Frese Jr, *J. Electroanal. Chem*., 1988, **245**, 223−244.

10 Y. Hori, *Electrochemical CO_2 reduction on metal electrodes, in Modern Aspects of Electrochemistry*, Springer, New York, 2008.

11 M. Gattrell, N. Gupta and A. Co, *J. Electroanal. Chem*., 2006, **594**, 1−19.

12 W. M. Ayers, *Carbon Dioxide Chemistry: Environmental Issues*, The Royal Society of Chemistry, U. K., 1994.

13 K. Ito, S. H. Ikeda and H. Noda, *Solar World Congress Proceedings Biennial Congress International Solar Energy Society*, Pergamon, Oxford, 1992.

14 R. L. Cook, R. C. MacDuff and A. F. Sammells, *J. Electrochem. Soc*., 1989, **136**, 1982−1984.

15 D. W. DeWulf, T. Jin and A. J. Bard, *J. Electrochem. Soc*., 1989, **136**, 1686−1691.

16 Y. Hori, A. Murata and R. Takahashi, *J. Chem. Soc., Faraday Trans.1*, 1989, **85**, 2309−2326.

17 Y. Hori, H. Wakebe, T. Tsukamoto, O. Koga, *Electrochim. Acta*., 1994, **39**, 1833−1839.

18 H. De Jesús-Cardona, C. del Moral and C. R. Cabrera, *J. Electroanal. Chem*., 2001, **513**, 45−51.

19 C. Delacourt, P. L. Ridgway, J. B. Kerr and J. Newman, *J. Electrochem. Soc*., 2008, **155**, B42−B49.

20 H. Noda, S. Ikeda, Y. Oda, and K. Ito, *Chem. Lett*., 1989, **18**, 289−292.

21 J. Krause, D. Borgmann and G. Wedler, *Surf. Sci*., 1996, **347**, 1−10.

22 I. A. Bonicke, W. Kirstein and F. Thieme, *Surf. Sci*., 1994, **307−309**, 177−181.

23 Y. Hori, A. Murata, T. Tsukamoto, H. Wakebe, O. Koga and H. Yamazaki, *Electrochim. Acta*., 1994, **39**, 2495−2500.

24 J. Pritchard, *Surf. Sci*., 1979, **79**, 231−244.

25 Y. Hori, O. Koga, H. Yamazaki and T. Matsuo, *Electrochim. Acta*., 1995, **40**, 2617−2622.

26 J. P. Perdew, K. Burke and M. Ernzerhof, *Phys. Rev. Lett*., 1996, **77**, 3865−3868.

27 D. Vanderbilt, *Phys. Rev. B*, 1990, **41**, 7892−7895.

28 M. Methfessel and A. T. Paxton, *Phys. Rev. B*, 1989, **40**, 3616−3621.

29 S. Baroni, A. Dal Corso, S. de Gironcoli and P. Giannozzi, PWSCF and PHONON: Plane-Wave Pseudo-Potential Codes. http://www.pwscf.org, 2001.

30 A. Kokalj, *J. Mol. Graph. Model*., 1999, **17**, 176−179.

31 A. Kokalj and M. Causà, *Scientific Visualization in Computational Quantum Chemistry*. *In Proceedings of High Performance Graphics Systems and Applications European Workshop*, CINECA-Interuniversity Consortium, Bologna, Italy, 2000.

32 A. Kokalj and M. Causà, XCrySDen: *X*-Window *CRY*stalline *S*tructures and *DEN*sities. http://www-k3.ijs.si/kokalj/xc/XCrySDen.html, 2001.

33 J. Greeley, A. A. Gokhale, J. Kreuser, J. A. Dumesic, H. Topsøe, N. Y. Topsøe and M. Mavrikakis, *J. Catal*., 2003, **213**, 63–72.

34 *CRC Handbook of Chemistry and Physics*, 91st edition (Internet Version 2011), CRC Press/Taylor and Francis, Boca Raton, FL, 2011.

35 G. Henkelman, and H. Jonsson, *J. Chem. Phys*., 2000, **113**, 9978−9985.

36 G. Henkelman, B. P. Uberuaga and H. Jonsson, *J. Chem. Phys.* 2000, **113**, 9901−9904.

37 A. A. Peterson, F. Abild-Pedersen, F. Studt, J. Rossmeisl and J. K. Nørskov, *Energy Environ. Sci*., 2010, **3**, 1311−1315.

38 W. J. Durand, A. A. Peterson, F. Studt, A. A. Peterson and J. K. Nørskov, *Surf. Sci*., 2011, **605**, 1354−1359.

39 Y. M. Choi and P. Liu, *J. Am. Chem. Soc*., 2009, **131**, 13054−13061.

40 A. Deluzarche, J. P. Hindermann, R. Kieffer, R. Breault and A. Kiennemann, *J. Phys. Chem.* 1984, **88**, 4993−4995.

41 A. Kiennemann, R. Breault, J. P. Hindermann and M. Laurin, *J. Chem. Soc., Faraday Trans. 1*, 1987, **83**, 2119−2128.

42 C. Diagne, H. Idriss, J. P. Hindermann and A. Kiennemann, *Appl. Catal*., 1989, **51**, 165−180.

43 I. N. Remediakis, F. Abild-Pedersen and J. K. Nørskov, *J. Phys. Chem. B*, 2004, **108**, 14535−14540.

44 J. K. Nørskov, J. Rossmeisl, A. Logadottir and L. Lindqvist, *J. Phys. Chem. B*, 2004, **108**, 17886−17892.

45 J. B. Hansen and P. E. Højlund Nielsen, Methanol synthesis, in *Handbook of Heterogeneous Catalysis*, ed. Ertl, G., Knözinger, H., Schüth, F., Weitkamp, J., volume 13, pp. 2920–2949. 2008.

46 K. J. P. Schouten, Y. Kwon, C. J. M. van der Ham, Z. Qin and M. T. M. Koper, *Chem. Sci*., 2011, **2**, 1902−1909.

47 K. J. P. Schouten, Z. Qin, E. P. Gallent and M. T. M. Koper, *J. Am. Chem. Soc*., 2012, **134**, 9864−9867.

48 M. Jitaru, D. A. Lowy, M. Toma, B. C. Toma and L. Oniciu, *J. Appl. Electrochem*., 1997, **27**, 875−889.

49 L. H. Ou, F. Yang, Y. W. Liu and S. L. Chen, *J. Phys. Chem. C*, 2009, **113**, 20657−20665.

50 J. Onsgaard, L. Bech, C. Svensgaard, P. J. Godowski and S. V. Hoffmann, *Prog. Surf. Sci*., 2001, **67**, 205−216.

Table of contents entry

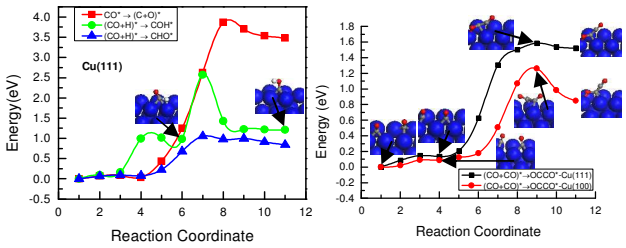

The research results have great significance for understanding in depth the selectivity of CO_2 electrochemical reduction process, and the sensitivity of surface structure.